TECHNISCHE MECHANIK, Band 24, Heft 1, (2004), 1-24
Manuskripteingang: 14. November 2003

Single-Plane Auto-Balancing of Rigid Rotors

L. Sperling, B. Ryzhik, H. Duckstein

This paper presents an analytical study of single-plane automatic balancing of statically and dynamically unbalanced rigid rotors, considering also the effect of partial unbalance compensation and vibration reduction. We consider a rotor equipped with a self- balancing device consisting of a circular track with moving balls to compensate for rotor unbalance. The investigations include an analysis of the equations of motion and determination of conditions for existence and stability of synchronous motions. Different solutions for the existence conditions correspond to different types of synchronous motions, including compensatory motions, with the elements' positions providing complete or partial compensation of unbalanced forces as well as reduction of vibrations. A stability analysis serves to determine the actual angular position of elements at any rotational speed and to find the speed range with stable unbalance compensation. Numerical simulations confirm the analytical results except for those in the immediate vicinity of critical speeds.

1 Introduction

In 1932, Thearle introduced a balancer system equipped with a pair of freely-moving balancing balls. Arranged at the plane of unbalance of a statically unbalanced rotor, the balls automatically gravitate towards the position, under specific conditions, that compensates for the unbalance. Since then, single-plane automatic balancing has become a well-known method. However, recently this method has attracted increased attention both from the theoretical point of view and from the application point of view. The method is advantageous, particularly for rotors with variable unbalance, such as washing machines, centrifuges, hand-held power tools, and CD-ROM drives.

A number of research groups in various countries are at present investigating this method in detail. Recently, several publications have revealed some important aspects of auto-balancing. The publication Chung and Ro (1999), for instance, analysed the dynamic stability and time response for an automatic single-plane balancer as a function of the system parameters. Kang et al. (2001) evaluated the performance of a ball-type balancer system installed in high-speed optical disk drives. The established mathematical model was analysed by the method of multiple scales. General design guidelines were suggested on the basis of possible steady-state solutions and the results of stability analyses. Huang and Chao (2002) also placed emphasis on the design of a ball-type balancer system for a high-speed disk drive and investigated the dependence of positional errors on the runway eccentricity, rolling resistance, and the drag force due to dynamic interaction between the ball and fluid-filled runway; the results of experiments were also discussed.

However, it is an established fact that a general rigid rotor has static and dynamic unbalances. Hence, in 1977 Hedaya and Sharp (1977) generalised the ball balancer device by proposing a device containing two planes with two balls each. Following the equations of motion, a stability analysis was presented and several relevant trends established from parametric studies. Similar results were also obtained by Inoe et al. (1979). In Bövik and Högfors (1986) the authors investigated an example of a non-planar rotor system facilitating the motion of two elements in the balancing device also in the axial direction.

The two-plane auto-balancing device for rigid rotors was further investigated by Sperling et al. They applied the method of direct separation of motion (see for example Blekhman, 2000) to develop the conditions for existence and stability of the balls' motion synchronous with that of the rotor. The corresponding stable phases were also determined. The results were confirmed and supplemented by computer simulation. Sperling et al. (2000) in which balls were treated as particles provided the first simple analytical result demonstrating the fact that compensation of both static and dynamic unbalances in the strongly post-critical range (where all spring forces may be neglected) is only possible for "long" rotors, i.e. those with a polar moment of inertia smaller than that about the transverse axis through the mass centre. This result was extended in Sperling et al. (2002) to the case of balls with a finite moment of inertia, rolling around the track without slipping. This publication included derivation of the full system of equations of motion, with non-rotating (but vibrating) masses also taken into account, an analytical approximation, and results of numerical simulations. Furthermore, it analysed the influence of system parameters, such as damping, on the operation of the device. Finally, a modified version of the Sommerfeld effect was demonstrated, whereby the balls attain motion at a speed corresponding to the rotor's

eigenfrequency. With the spring forces also being taken into account the analytical part of the paper by Sperling et al. (2001) shows that full compensation of rotor unbalances is possible only for rotors with a polar moment of inertia smaller than the transverse one (i.e. for rotors with a second critical speed) in the frequency range beyond the second critical speed. Simulations illustrate the rotor run-up to nominal speed, whereby full unbalance compensation is achieved.
The conditions for full unbalance compensation by means of the above-mentioned two-plane balancing devices cause major restrictions for applying the method in practice. Therefore, the present paper is dedicated to the potential of partial unbalance compensation, namely at first only using a single-plane device. The differential equations of motion are employed for a model rotor with n balls distributed on any number of planes to derive the general conditions of existence and stability for the balls' motions synchronous with the rotor's angular speed. Various cases of partial compensation using single-plane balancers are investigated and discussed. In particular, the investigation revealed that, under certain conditions, auto-balancing devices can reduce the apparent unbalances and vibrations within a frequency range beyond the first critical speed, even if the rotor's polar moment of inertia exceeds the transverse one.
The results of the analytical investigation were verified by numerical simulations for rotor speeds at sufficient distance from the critical speeds. For the areas near critical speeds, the simulations show typical non-synchronous transient motions, which, as a rule, excite increased vibrations.

2 Model

Fig. 1 shows a rigid rotor with a single-plane auto-balancing device. The axisymmetric rotor has mass m_R and moments of inertia $J_{xxR} = J_{yyR} = J_{aR}$, $J_{zzR} = J_{zR}$, $J_{xyR} = J_{yzR} = J_{zxR} = 0$ with respect to the centre of mass S in the non-rotating vector frame $\vec{e}_x, \vec{e}_y, \vec{e}_z$, whereas $\mathbf{q}_V = [\, r_x \quad \psi_y \quad r_y \quad \psi_x \,]^{\mathrm{T}}$ are the coordinates of the vibrational motion (see Fig. 2 a). The rotor has m unbalances in the planes z_k, ($k = n + 1,\ldots, n + m$), hereafter referred to as inherent unbalances, idealised as particles with masses m_k and eccentricities ε_κ. The angular velocity of the rotor is $\dot{\varphi}_R$; the angular positions of the inherent unbalances are $\varphi_k = \varphi_R + \alpha_\kappa$, $k = n + 1,\ldots, n + m$.
As long as our aim is to consider, eventually, various types of devices, we assume that the general device model contains n identical balls distributed within any number of planes (maximum number n). The balls are characterised by the masses m_i, the radii r_i, the eccentricities ε_i and the plane positions z_i, $i = 1,\ldots, n$. The motion of the balls in the auto-balancing planes is described by the angular coordinates φ_i and ϑ_i, $i = 1,\ldots, n$ (see Figs. 1 and 2 b). Assuming that the balls roll around the tracks without slipping (see Fig. 2 b), we may write

$$\dot{\vartheta}_i = \frac{1}{r_i}\left(R_i\dot{\varphi}_R - \varepsilon_i\dot{\varphi}_i\right), \qquad R_i = \varepsilon_i + r_i, \qquad i = 1,\ldots,n\,. \tag{1}$$

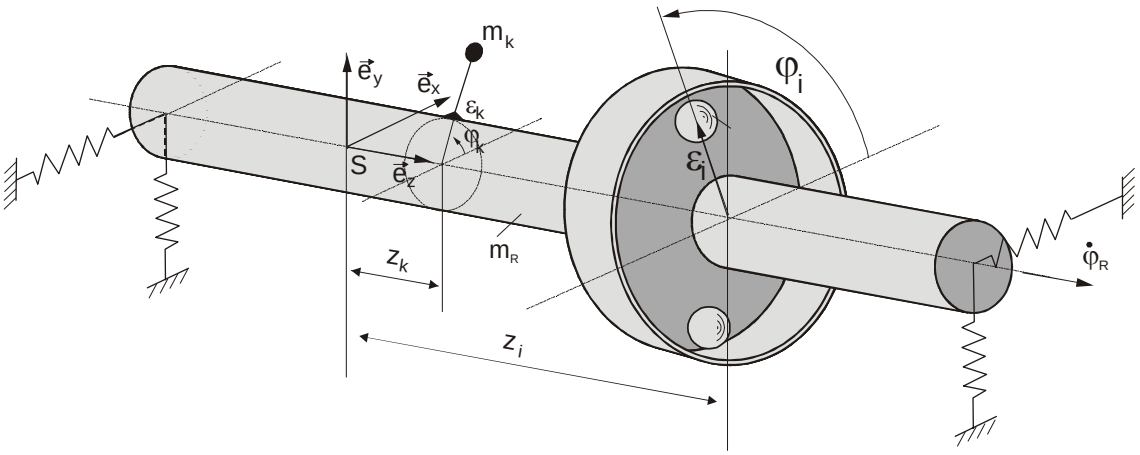

Figure 1. Rigid rotor with a single-plane auto-balancing device

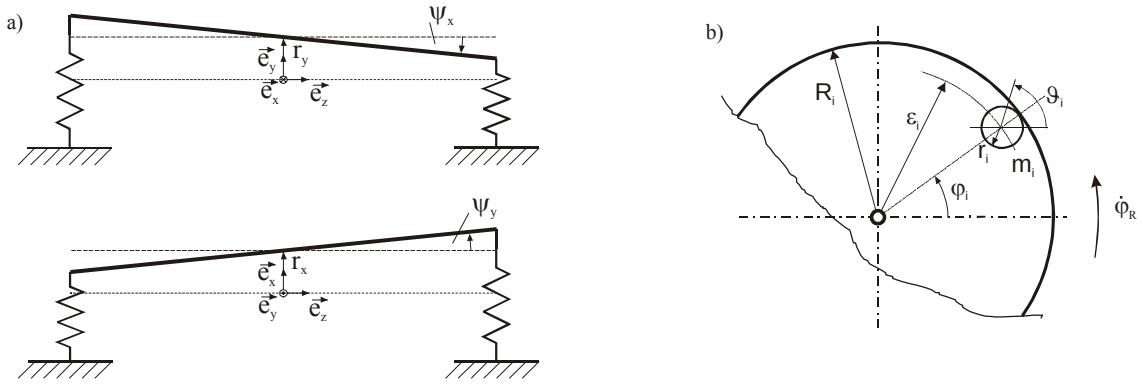

Figure 2. Main system variables

The damping moment caused by the viscous medium acting on the ball is

$$l_i = d_i\left(\dot{\vartheta}_i - \dot{\varphi}_R\right) = d_i \frac{\varepsilon_i}{r_i}\left(\dot{\varphi}_R - \dot{\varphi}_i\right), \tag{2}$$

with d_i resulting from the viscosity of the medium. The corresponding generalised "forces" for the rotor and ball are the moments

$$Q_{Ri} = -\beta_i\left(\dot{\varphi}_R - \dot{\varphi}_i\right), \qquad Q_i = \beta_i\left(\dot{\varphi}_R - \dot{\varphi}_i\right), \qquad \text{where } \beta_i = d_i\left(\frac{\varepsilon_i}{r_i}\right)^2. \tag{3}$$

Taking external damping also into account , the overall damping moment acting upon the rotor is

$$M_d = -\left[\overline{\beta}_R\dot{\varphi}_R + \sum_{i=1}^{n}\beta_i\left(\dot{\varphi}_R - \dot{\varphi}_i\right)\right] = -\beta_R\dot{\varphi}_R + \sum_{i=1}^{n}\beta_i\dot{\varphi}_i\,, \qquad \text{where } \beta_R = \overline{\beta}_R + \sum_{i=1}^{n}\beta_i\,. \tag{4}$$

3 Equations of Motion

The rotor is assumed to be mounted on two isotropic elastic damped supports with stiffnesses k_{11}, k_{12}, k_{22} and damping factors c_{11}, c_{12}, c_{22} with respect to the vibrational co-ordinates $\mathbf{q}_V$.
Using the abbreviations

$$M = m_R + \sum_{i=1}^{n+m} m_i\,, \qquad J_{bi} = \frac{2}{5}m_i r_i^{\,2}\,, \qquad i = 1,\ldots,n\,, \tag{5}$$

$$J_a = J_{aR} + \sum_{i=1}^{n+m} m_i z_i^2 + \sum_{i=1}^{n} J_{bi}\,, \qquad J_z = J_{zR} + \sum_{i=1}^{n}\left(\frac{R_i}{r_i}\right)^2 J_{bi} + \sum_{\mathrm{i=n+1}}^{\mathrm{n+m}} m_{\mathrm{i}}\varepsilon_i^{\,2}\,, \tag{6}$$

$$\widetilde{J}_z = J_{zR} + \sum_{i=1}^{n}\frac{R_i}{r_i}J_{bi}\,, \qquad \widetilde{J}_i = \begin{cases} m_i\varepsilon_i\left(\varepsilon_i - \dfrac{2}{5}r_i\right), & i = 1,\ldots,n, \\ m_i\varepsilon_i^{\,2}, & i = m+1,\ldots,n+m, \end{cases} \tag{7}$$

$$J_i = \frac{7}{5}m_i\varepsilon_i^{\,2}, \qquad J_{iR} = \frac{R_i\varepsilon}{r_i^2}J_{bi}\,, \qquad i = 1,\ldots,n \tag{8}$$

and including the rotor driving torque $L_R = L_R\left(\dot{\varphi}_R\right)$, we obtain the following Lagrange's equations for the system under investigation, linearised in the vibrational co-ordinates $\mathbf{q}_V$ (see Sperling et al., 2002)

$$M\ddot{r}_x + \sum_{k=1}^{n+m} m_k z_k \ddot{\psi}_y + c_{11}\dot{r}_x + c_{12}\dot{\psi}_y + k_{11} r_x + k_{12}\psi_y = \sum_{k=1}^{n+m} m_k \varepsilon_k \left(\ddot{\varphi}_k \sin\varphi_k + \dot{\varphi}_k^2 \cos\varphi_k\right), \tag{9}$$

$$\begin{aligned}
&\sum_{k=1}^{n+m} m_k z_k \ddot{r}_x + J_a \ddot{\psi}_y + \tfrac{1}{2}\sum_{k=1}^{n+m} m_k \varepsilon_k^2 \left[-\ddot{\psi}_x \sin 2\varphi_k + \ddot{\psi}_y \left(1+\cos 2\varphi_k\right)\right] \\
&+ c_{12}\dot{r}_x + c_{22}\dot{\psi}_y - \left[\widetilde{J}_z \dot{\varphi}_R + \sum_{k=1}^{n+m} \widetilde{J}_k \dot{\varphi}_k\right]\dot{\psi}_x - \sum_{k=1}^{n+m} m_k \varepsilon_k^2 \dot{\varphi}_k \left(\dot{\psi}_x \cos 2\varphi_k + \dot{\psi}_y \sin 2\varphi_k\right) \\
&+ k_{12} r_x + k_{22}\psi_y - \tfrac{1}{2}\left[\widetilde{J}_z \ddot{\varphi}_R + \sum_{k=1}^{n+m} \widetilde{J}_k \ddot{\varphi}_k\right]\psi_x = \sum_{k=1}^{n+m} m_k \varepsilon_k z_k \left(\ddot{\varphi}_k \sin\varphi_k + \dot{\varphi}_k^2 \cos\varphi_k\right),
\end{aligned} \tag{10}$$

$$M\ddot{r}_y - \sum_{k=1}^{n+m} m_k z_k \ddot{\psi}_x + c_{11}\dot{r}_y - c_{12}\dot{\psi}_x + k_{11} r_y - k_{12}\psi_x = -\sum_{k=1}^{n+m} m_k \varepsilon_k \left(\ddot{\varphi}_k \cos\varphi_k - \dot{\varphi}_k^2 \sin\varphi_k\right), \tag{11}$$

$$\begin{aligned}
&-\sum_{k=1}^{n+m} m_k z_k \ddot{r}_y + J_a \ddot{\psi}_x + \tfrac{1}{2}\sum_{k=1}^{n+m} m_k \varepsilon_k^2 \left[\ddot{\psi}_x \left(1-\cos 2\varphi_k\right) - \ddot{\psi}_y \sin 2\varphi_k\right] \\
&- c_{12}\dot{r}_y + c_{22}\dot{\psi}_x + \left[\widetilde{J}_z \dot{\varphi}_R + \sum_{k=1}^{n+m} \widetilde{J}_k \dot{\varphi}_k\right]\dot{\psi}_y + \sum_{k=1}^{n+m} m_k \varepsilon_k^2 \dot{\varphi}_k \left(\dot{\psi}_x \sin 2\varphi_k - \dot{\psi}_y \cos 2\varphi_k\right) \\
&- k_{12} r_y + k_{22}\psi_x + \tfrac{1}{2}\left[\widetilde{J}_z \ddot{\varphi}_R + \sum_{k=1}^{n+m} \widetilde{J}_k \ddot{\varphi}_k\right]\psi_y = \sum_{k=1}^{n+m} m_k \varepsilon_k z_k \left(\ddot{\varphi}_k \cos\varphi_k - \dot{\varphi}_k^2 \sin\varphi_k\right),
\end{aligned} \tag{12}$$

$$J_z\ \ddot{\varphi}_{\mathrm{R}} - \sum_{\mathrm{k=1}}^{\mathrm{n}} J_{kR}\ddot{\varphi}_{\mathrm{k}} + \beta_{\mathrm{R}}\dot{\varphi}_{\mathrm{R}} - \sum_{\mathrm{k=1}}^{\mathrm{n}} \beta_k \dot{\varphi}_{\mathrm{k}} - \sum_{\mathrm{k=n+1}}^{\mathrm{n+m}} \mathrm{m_k}\varepsilon_{\mathrm{k}}\left[\ddot{r}_{kx}\ \sin\varphi_{\mathrm{k}} - \ddot{r}_{ky}\ \cos\varphi_{\mathrm{k}}\right] = \mathrm{L_R}\left(\dot{\varphi}_{\mathrm{R}}\right), \tag{13}$$

$$-J_{iR}\ddot{\varphi}_R + J_i\ddot{\varphi}_i - \beta_i\dot{\varphi}_R + \beta_i\dot{\varphi}_i - m_i\varepsilon_i\left[\ddot{r}_{ix}\ \sin\varphi_i - \ddot{r}_{iy}\ \cos\varphi_i\right] = 0, \qquad i = 1,...,n \tag{14}$$

with

$$r_{ix} = r_x + z_i\psi_y, \quad r_{iy} = r_y - z_i\psi_x, \qquad i = 1,...,n+m\,. \tag{15}$$

4 General Conditions for Existence and Stability of the Balls' Motions Synchronous with the Rotor's Angular Speed

Assuming a constant rotor angular velocity $\dot{\varphi}_R = \Omega = const.$, the equations of motion of the balls (14) become

$$J_i\ddot{\varphi}_i + \beta_i\dot{\varphi}_i + B_i = \beta_i\Omega\,, \qquad B_i = -m_i\varepsilon_i\left[\ddot{r}_{ix}\sin\varphi_i - \ddot{r}_{iy}\cos\varphi_i\right], \quad i = 1,...,n\,. \tag{16}$$

Following the method of direct separation of motion we suppose

$$\varphi_i(t) = \Omega t + \alpha_i(t) + \xi_i\left(t,\Omega,\right), \quad i = 1,...,n \tag{17}$$

with the slowly varying term $\alpha_i(t)$, $\dot{\alpha}_i(t) << \Omega$, and the 2π - periodic fast term $\xi_i\left(t,\Omega t\right)$ with a vanishing average over a period of the "fast time" Ωt.
Thus, Eq. (16) yields

$$J_i\ddot{\alpha}_i + \beta_i\dot{\alpha}_i + V_i = 0, \qquad i = 1,...,n \tag{18}$$

with the so-called vibrational moments

$$V_i = \frac{1}{2\pi}\int_0^{2\pi} B_i\, d\left(\Omega t\right), \tag{19}$$

where

$$B_i = -m_i\varepsilon_i\left[\ddot{r}_{ix}\sin(\Omega t+\alpha_i)-\ddot{r}_{iy}\cos(\Omega t+\alpha_i)\right],\quad i=1,...,n. \tag{20}$$

To obtain an approximation for steady-state vibrations we neglect the unbalance masses and inertia moments as well as the damping terms in Eqs. (9) - (12), and substitute Eq. (17) neglecting fast terms to get (with J_z instead of $\widetilde{J}_z$ to simplify notation)

$$M\ddot{r}_x + k_{11}r_x + k_{12}\psi_y = \sum_{k=1}^{n+m} f_k\cos(\Omega t+\alpha_k), \tag{21}$$

$$J_a\ddot{\psi}_y - J_z\Omega\dot{\psi}_x + k_{12}r_x + k_{22}\psi_y = \sum_{k=1}^{n+m} z_k f_k\cos(\Omega t+\alpha_k) \tag{22}$$

$$M\ddot{r}_y + k_{11}r_y - k_{12}\psi_x = \sum_{k=1}^{n+m} f_k\sin(\Omega t+\alpha_k), \tag{23}$$

$$J_a\ddot{\psi}_x + J_z\Omega\dot{\psi}_y - k_{12}r_y + k_{22}\psi_x = -\sum_{k=1}^{n+m} z_k f_k\sin(\Omega t+\alpha_k) \tag{24}$$

with the centrifugal forces

$$f_i = m_i\varepsilon_i\Omega^2,\ i=1,...,n+m. \tag{25}$$

Eqs. (21) – (24) yield the stationary orbital motion of the centres of the circular ball paths

$$r_{ix} = \sum_{k=1}^{n+m} f_k A_{ik}\cos(\Omega t+\alpha_k), \qquad r_{iy} = \sum_{k=1}^{n+m} f_k A_{ik}\sin(\Omega t+\alpha_k) \tag{26}$$

or

$$r_{ix} = r_{i\xi}\cos\Omega t - r_{i\eta}\sin\Omega t,\quad r_{iy} = r_{i\eta}\cos\Omega t + r_{i\xi}\sin\Omega t \tag{27}$$

with the components in a frame ξ,η rotating with the rotor

$$r_{i\xi} = \sum_{k=1}^{n+m} f_k A_{ik}\cos\alpha_k, \qquad r_{i\eta} = \sum_{k=1}^{n+m} f_k A_{ik}\sin\alpha_k, \qquad i=1,...,n \tag{28}$$

and the harmonic influence coefficients

$$A_{ik} = \frac{1}{\Delta}\left\{-(J_a-J_z)\Omega^2 + k_{22} - k_{12}z_k + z_i\left[\left(-M\Omega^2+k_{11}\right)z_k - k_{12}\right]\right\}, \tag{29}$$

where

$$\Delta = M(J_a-J_z)\Omega^4 - \left[Mk_{22} + (J_a-J_z)k_{11}\right]\Omega^2 + k_{11}k_{22} - {k_{12}}^2. \tag{30}$$

Thus, we obtain from Eqs. (19), (20), (26), (27)

$$V_i = B_i = f_i\sum_{k=1}^{n+m} f_k A_{ik}\sin(\alpha_i-\alpha_k) = f_i\left(r_{i\xi}\sin\alpha_i - r_{i\eta}\cos\alpha_i\right),\ i=1,...,n. \tag{31}$$

The balls' synchronous motions of interest have constant phases $\alpha_i = \alpha_i^*$, $i=1,...,n$. Hence, the existence conditions for such motions, following from Eqs. (18) and (31), are

$$V_i\left(\alpha_1=\alpha_1^*,...,\alpha_n=\alpha_n^*\right) = f_i\sum_{k=1}^{n+m} f_k A_{ik}\sin\left(\alpha_i^*-\alpha_k^*\right) = 0,\ i=1,...,n, \tag{32}$$

where $\alpha_i^* \equiv \alpha_i$, $i = n+1,...,n+m$.
Obviously, because of Eq. (31), one solution type of the existence conditions (32) is determined by the conditions

$$r_{i\xi} = 0\,, \qquad r_{i\eta} = 0\,, \qquad i = 1,...,n\,, \tag{33}$$

for which, from Eq. (27), immediately follows

$$r_{ix} = 0\,, \qquad r_{iy} = 0\,. \qquad i = 1,...,n\,. \tag{34}$$

This means that for this type of solutions the centres of the device planes remain at rest. Therefore, we call this type of solutions "compensation type solution". Notice that in the case of a single-plane device this type of solutions only ensures the disappearance of vibrations in the plane of the device, while in the case of a two-plane device the compensation of the unbalances is complete and vibrations are theoretically equal to zero for the whole rotor.
To evaluate the stability of the various solutions to Eq. (32), the equations in variations

$$J_i\ddot{\overline{\alpha}}_i + \beta_i\dot{\overline{\alpha}}_i + f_i\left[\sum_{k=1}^{n} f_k A_{ik}\cos\left(\alpha_i^* - \alpha_k^*\right)\left(\overline{\alpha}_i - \overline{\alpha}_k\right) + \overline{\alpha}_i\sum_{k=n+1}^{n+m} f_k A_{ik}\cos\left(\alpha_i^* - \alpha_k\right)\right] = 0, \qquad i = 1,...,n \tag{35}$$

following from Eqs. (18) and (32) need to be analysed. Substitution of Eq. (33) under consideration of Eq. (28) yields the following simpler form of the equations in variations for solutions of compensating type

$$J_i\ddot{\overline{\alpha}}_i + \beta_i\dot{\overline{\alpha}}_i - f_i\sum_{k=1}^{n} f_k A_{ik}\cos\left(\alpha_i^* - \alpha_k^*\right)\overline{\alpha}_k = 0\,. \tag{36}$$

Assuming that $\beta_i > 0$, $i = 1,\ldots, n$, the positive definiteness of the "stiffness matrix" of Eq. (35) (or of Eq. (36) in the special case of compensating solutions) is a necessary and sufficient condition for the asymptotic stability of any solution of Eq. (32).
We can suggest also another view on compensation conditions, writing instead of Eq. (28)

$$r_{i\xi} = \sum_{k=1}^{n} f_k A_{ik}\cos\alpha_k + \hat{r}_{i\xi}\,, \qquad r_{i\eta} = \sum_{k=1}^{n} f_k A_{ik}\sin\alpha_k + \hat{r}_{i\eta}\,, \qquad i = 1,...,n\,, \tag{37}$$

where

$$\hat{r}_{i\xi} = \hat{r}_i\cos\hat{\alpha}_i = \sum_{k=n+1}^{n+m} f_k A_{ik}\cos\alpha_k\,, \qquad \hat{r}_{i\eta} = \hat{r}_i\sin\hat{\alpha}_i = \sum_{k=n+1}^{n+m} f_k A_{ik}\sin\alpha_k\,. \tag{38}$$

To definitely determine $\hat{\alpha}_i$ we predefine $\hat{r}_i > 0$. Specifically, $\hat{r}_i$ is the constant rotating displacement in the plane of the i-th ball, caused by the inherent (primary) static and dynamic rotor unbalances as a whole.
Hence, the existence conditions for synchronous motions are

$$\sum_{k=1}^{n} f_k A_{ik}\sin\left(\alpha_i^* - \alpha_k^*\right) + \hat{r}_i\sin\left(\alpha_i^* - \hat{\alpha}_i\right) = 0\,, \qquad i = 1,...,n\,. \tag{39}$$

Because of

$$\sum_{k=n+1}^{n+m} f_k A_{ik}\cos\left(\alpha_i^* - \alpha_k\right) = \hat{r}_i\cos\left(\alpha_i^* - \hat{\alpha}_i\right), \tag{40}$$

we obtain from Eq. (35) the alternative form of the equations in variations

$$J_i\ddot{\overline{\alpha}}_i + \beta_i\dot{\overline{\alpha}}_i + f_i\left[\sum_{k=1}^{n} f_k A_{ik}\cos\left(\alpha_i^* - \alpha_k^*\right)\left(\overline{\alpha}_i - \overline{\alpha}_k\right) + \overline{\alpha}_i\hat{r}_i\cos\left(\alpha_i^* - \hat{\alpha}_i\right)\right] = 0, \qquad i = 1,...,n. \tag{41}$$

We would like to point out that the solutions of the existence and stability conditions are valid only at a sufficient distance from the critical rotor speed.

5 Single-plane Balancer

5.1 A Single Ball

A single ball alone is not able to guarantee a solution of the compensation conditions.
The existence condition, following from Eq. (39),

$$\hat{r}_1 \sin\left(\alpha_1^* - \hat{\alpha}_1\right) = 0 \tag{42}$$

has only the two solutions

$$\alpha_1^* = \hat{\alpha}_1 , \qquad \alpha_1^* = \hat{\alpha}_1 + \pi . \tag{43}$$

The equation in variation

$$J_1 \ddot{\overline{\alpha}}_1 + \beta_1 \dot{\overline{\alpha}}_1 + f \hat{r}_1 \cos\left(\alpha_1^* - \hat{\alpha}_1\right) \overline{\alpha}_1 = 0 , \tag{44}$$

where f is the centrifugal force of the ball, yields the stability condition

$$\cos\left(\alpha_1^* - \hat{\alpha}_1\right) > 0 . \tag{45}$$

Thus, the solution $\alpha_1^* = \hat{\alpha}_1$ is always stable (see Fig. 3), and the solution $\alpha_1^* = \hat{\alpha}_1 + \pi$ is always unstable (see Fig. 4). This means that the ball always follows the vibration in the plane of the device, i.e. the angular position of the ball coincides with the phase of vibration, because according to Eqs. (39) and (42) the vibrational moment engendered by the ball is zero.

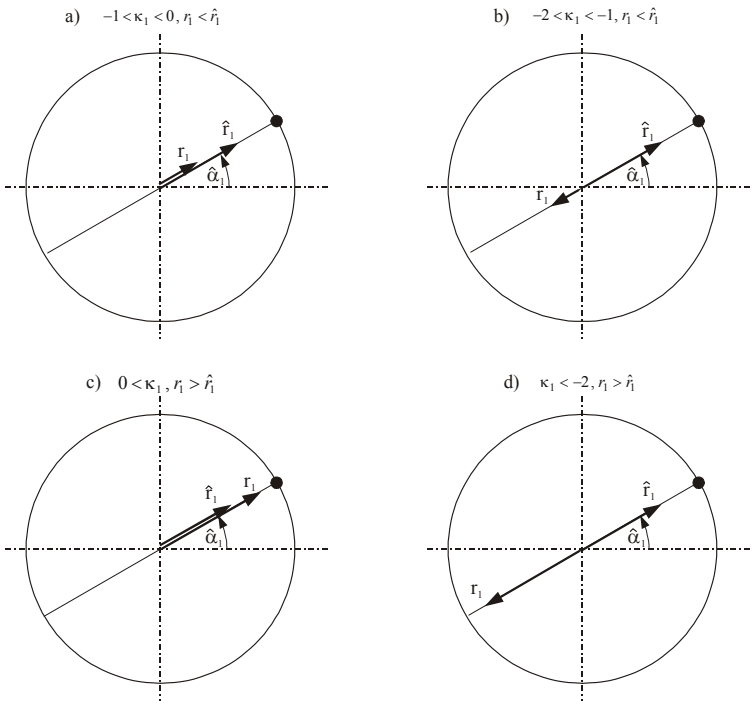

Figure 3. Different cases of stable ball position for a single-ball device.

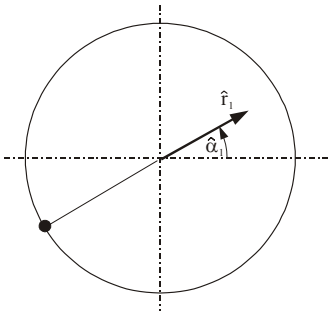

Figure 4. Unstable ball position for a single-ball device

For the stable solution we obtain

$$r_{1\xi} = \left(fA_{11} + \hat{r}_1\right)\cos\hat{\alpha}_1 , \qquad r_{1\eta} = \left(fA_{11} + \hat{r}_1\right)\sin\hat{\alpha}_1 , \tag{46}$$

$$r_1 = \sqrt{{r_{i\xi}}^2 + {r_{i\eta}}^2} = \left|fA_{11} + \hat{r}_1\right| . \tag{47}$$

The condition for decreasing vibrations in the plane of the device is

$$\left|fA_{11} + \hat{r}_1\right| < \hat{r}_1$$

or

$$-\frac{2\hat{r}_1}{f} < A_{11} < 0\,. \tag{48}$$

Introducing the function

$$\kappa_1(\Omega) = \frac{fA_{11}(\Omega)}{\hat{r}_1(\Omega)} = \frac{r_1^b(\Omega)}{\hat{r}_1(\Omega)}, \tag{49}$$

where

$$r_1^b(\Omega) = fA_{11}(\Omega) \tag{50}$$

is the signed deflection caused by the force *f,* we obtain the condition for stable decreasing of the vibration due to the single-plane self-balancing device with a single ball in the form (see Fig. 3 a) and b))

$$-2 < \kappa_1(\Omega) < 0\,. \tag{51}$$

Within other ranges of rotational speed the vibrations will increase (see Fig. 3 c) and d)).

5.2 Single-plane Device with Two Identical Balls

In the case of a single-plane device ($z_2 = z_1$, $A_{2i} = A_{1i}$, $i = 1,...,2+m$, $\hat{r}_2 = \hat{r}_1$, $\hat{\alpha}_2 = \hat{\alpha}_1$) with two identical balls ($f_1 = f_2 = f$), the existence conditions for compensatory solutions (33) may be rewritten as

$$\begin{aligned} r_{1\xi} &= fA_{11}\left(\cos\alpha_1^* + \cos\alpha_2^*\right) + \hat{r}_1\cos\hat{\alpha}_1 = 0, \\ r_{1\eta} &= fA_{11}\left(\sin\alpha_1^* + \sin\alpha_2^*\right) + \hat{r}_1\sin\hat{\alpha}_1 = 0 \end{aligned} \tag{52}$$

or

$$\begin{aligned} &\cos\left(\alpha_1^* - \hat{\alpha}_1\right) + \cos\left(\alpha_2^* - \hat{\alpha}_1\right) = -\frac{\hat{r}_1}{fA_{11}}, \\ &\sin\left(\alpha_1^* - \hat{\alpha}_1\right) + \sin\left(\alpha_2^* - \hat{\alpha}_1\right) = 0 \end{aligned} \tag{53}$$

with the only solution

$$\alpha_1^* = \hat{\alpha}_1 + \gamma\,, \qquad \alpha_2^* = \hat{\alpha}_1 - \gamma\,, \qquad \gamma = \arccos\left(-\frac{\hat{r}_1}{2fA_{11}}\right). \tag{54}$$

This solution exists only if

$$\left|\frac{\hat{r}_1}{2fA_{11}}\right| \le 1\,. \tag{55}$$

The equations in variations (36) become

$$J_i\ddot{\overline{\alpha}}_i + \beta_i\dot{\overline{\alpha}}_i - f^2A_{11}\sum_{k=1}^{2}\cos\left(\alpha_i^* - \alpha_k^*\right)\overline{\alpha}_k = 0\,. \tag{56}$$

Thus, the "stiffness matrix" for these equations is

$$\mathbf{S} = -f^2A_{11}\begin{bmatrix} 1 & \cos\left(\alpha_1^* - \alpha_2^*\right) \\ \cos\left(\alpha_1^* - \alpha_2^*\right) & 1 \end{bmatrix} \tag{57}$$

with the determinant

$$\det\mathbf{S} = f^4{A_{11}}^2\sin^2\left(\alpha_1^* - \alpha_2^*\right). \tag{58}$$

Under the condition $\sin\left(\alpha_1^* - \alpha_2^*\right) \neq 0$, Eq. (58) yields $\det \mathbf{S} > 0$, and we obtain the necessary and sufficient stability condition

$$A_{11} = \frac{1}{\Delta}\left[-\left(J_a - J_z\right)\Omega^2 + k_{22} - \left(M\Omega^2 - k_{11}\right)z_1{}^2 - 2k_{12}z_1\right] < 0\,. \tag{59}$$

Introducing the function

$$\kappa_2 = \frac{2fA_{11}(\Omega)}{\hat{r}_1(\Omega)} = 2\frac{r_1^b(\Omega)}{\hat{r}_1(\Omega)} \tag{60}$$

this condition, together with condition (55), yields (see Fig. 5 b))

$$\kappa_2(\Omega) \leq -1\,. \tag{61}$$

In the special case of only static concentrated inherent unbalance in the device plane, the inequality $A_{11} < 0$ (see Eq. (59)) means that the direction of $\hat{r}_1$ is opposite to that of the centrifugal force due to inherent unbalance.
All other solutions of the general existence conditions

$$\begin{aligned} fA_{11}\sin\left(\alpha_1^* - \alpha_2^*\right) + \hat{r}_1\sin\left(\alpha_1^* - \hat{\alpha}_1\right) &= 0, \\ fA_{11}\sin\left(\alpha_2^* - \alpha_1^*\right) + \hat{r}_1\sin\left(\alpha_2^* - \hat{\alpha}_1\right) &= 0, \end{aligned} \tag{62}$$

are of the type $\sin\left(\alpha_1^* - \alpha_2^*\right) = 0$.
The general equations in variations (41) are

$$\begin{aligned} &J_1\ddot{\overline{\alpha}}_1 + \beta_1\dot{\overline{\alpha}}_1 + f\left[fA_{11}\cos\left(\alpha_1^* - \alpha_2^*\right)\left(\overline{\alpha}_1 - \overline{\alpha}_2\right) + \hat{r}_1\cos\left(\alpha_1^* - \hat{\alpha}_1\right)\overline{\alpha}_1\right], \\ &J_2\ddot{\overline{\alpha}}_2 + \beta_2\dot{\overline{\alpha}}_2 + f\left[fA_{11}\cos\left(\alpha_2^* - \alpha_1^*\right)\left(\overline{\alpha}_2 - \overline{\alpha}_1\right) + \hat{r}_1\cos\left(\alpha_2^* - \hat{\alpha}_1\right)\overline{\alpha}_2\right]. \end{aligned} \tag{63}$$

a) Solution $\alpha_1^* = \hat{\alpha}_1, \quad \alpha_2^* = \hat{\alpha}_1$

The components (37) in the rotating frame become

$$r_{1\xi} = \left(2fA_{11} + \hat{r}_1\right)\cos\hat{\alpha}_1\,, \qquad r_{1\eta} = \left(2fA_{11} + \hat{r}_1\right)\sin\hat{\alpha}_1\,. \tag{64}$$

Hence,

$$r_1 = \sqrt{r_{i\xi}{}^2 + r_{i\eta}{}^2} = \left|2fA_{11} + \hat{r}_1\right|. \tag{65}$$

The vibrations decrease, when $A_{11} < 0$ and $\kappa_2(\Omega) > -1$
or (see Fig. 5 a))

$$-1 < \kappa_2(\Omega) < 0\,. \tag{66}$$

Compared to condition (61), this condition means that the ball masses are insufficient to completely compensate the inherent unbalance.
The stiffness matrix for the equations in the variations becomes

$$\mathbf{S} = f\begin{bmatrix} fA_{11} + \hat{r}_1 & -fA_{11} \\ -fA_{11} & fA_{11} + \hat{r}_1 \end{bmatrix}. \tag{67}$$

The considered solution is stable if

$$fA_{11} + \hat{r}_1 > 0 \qquad \text{and} \qquad \hat{r}_1\left(2fA_{11} + \hat{r}_1\right) > 0 \tag{68}$$

or if $\quad 2fA_{11} + \hat{r}_1 > 0\,,$ (69)

i. e.

$$\kappa_2(\Omega) > -1\,. \tag{70}$$

Hence, the case (66) with decreasing vibrations is always stable. However, the position of the balls, determined by the condition $0 < \kappa_2$ and causing increased vibrations, is also stable (see Fig. 5 c)).

b) Solution $\alpha_1^* = \hat{\alpha}_1 + \pi, \quad \alpha_2^* = \hat{\alpha}_1 + \pi$

The stiffness matrix for the equations in the variations becomes

$$\mathbf{S} = f\begin{bmatrix} fA_{11} - \hat{r}_1 & -fA_{11} \\ -fA_{11} & fA_{11} - \hat{r}_1 \end{bmatrix}. \tag{71}$$

The stability conditions

$$fA_{11} - \hat{r}_1 > 0\,, \qquad -\hat{r}_1\left(2fA_{11} - \hat{r}_1\right) > 0\,, \tag{72}$$

contradict each other. Thus, this type of ball motion is always unstable (see Fig. 6 a).

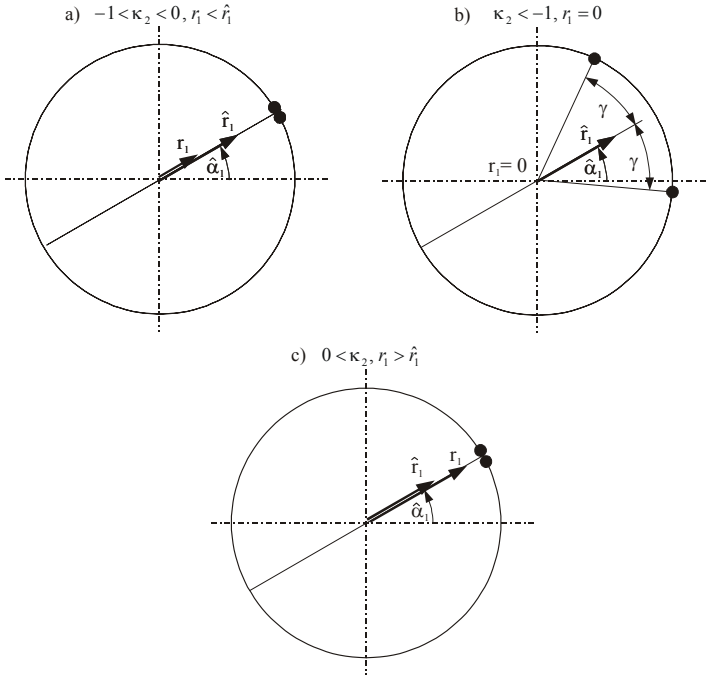

Figure 5. Different cases of stable positions of the balls for a two-ball device.

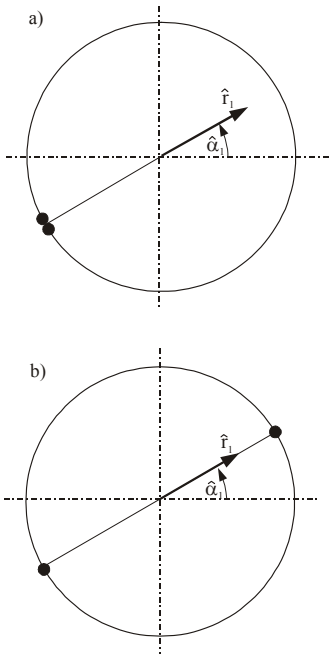

Figure 6. Unstable positions of the balls for a two-ball device.

c) Solution $\alpha_1^* = \hat{\alpha}_1 + \pi, \quad \alpha_2^* = \hat{\alpha}_1$ (or $\alpha_1^* = \hat{\alpha}_1, \quad \alpha_2^* = \hat{\alpha}_1 + \pi$)

The stiffness matrix for the equations in the variations becomes

$$\mathbf{S} = f\begin{bmatrix} -fA_{11} + \hat{r}_1 & fA_{11} \\ fA_{11} & -fA_{11} - \hat{r}_1 \end{bmatrix}. \tag{73}$$

This matrix is positive definite, when

$$-fA_{11} + \hat{r}_1 > 0\,, \qquad -\hat{r}_1^{\,2} > 0\,. \tag{74}$$

Because the second condition is impossible, this type of motion is also always unstable (see Fig. 6 b).

6 Investigation of the Condition $A_{11} < 0$

For the rigid rotor that in general is both statically and dynamically unbalanced and has a single-plane self-balancing device (at $z = z_1$) a survey will be made of the various cases of satisfying the stability condition (59),

$$-A_{11} = \frac{N_1}{\Delta} > 0 \ , \tag{75}$$

for the phasing of two balls, for which the vibrations in the balancing plane will be compensated - either completely or, for balls of insufficient mass, partially (see Eq. (66)). This is at the same time the necessary condition for decreasing vibrations by means of only a single ball (see Eq. (48)). The following formulae and graphics should assist engineers involved in automatic balancing of rotors in classifying their specific rotors and designing appropriate balancing devices.
The denominator and numerator in (75) are

$$\Delta = M\left(J_a - J_z\right)\Omega^4 - \left[Mk_{22} + \left(J_a - J_z\right)k_{11}\right]\Omega^2 + k_{11}k_{22} - {k_{12}}^2 , \tag{76}$$

$$N_1 = \left(J_a - J_z\right)\Omega^2 - k_{22} + \left(M\,\Omega^2 - k_{11}\right){z_1}^2 + 2k_{12}z_1 . \tag{77}$$

Introducing the square of the "rotational critical speed"

$${\Omega_r}^2 = \frac{k_{22}}{J_a - J_z} , \tag{78}$$

the square of the "translational critical speed"

$${\Omega_t}^2 = \frac{k_{11}}{M} , \tag{79}$$

and the square of the "interactional speed"

$$\overline{\Omega}^2 = \frac{k_{12}}{\sqrt{M\left(J_a - J_z\right)}} , \tag{80}$$

we obtain

$$\Delta = M\left(J_a - J_z\right)\left[\left(\Omega^2 - {\Omega_r}^2\right)\left(\Omega^2 - {\Omega_t}^2\right) - \overline{\Omega}^4\right] , \tag{81}$$

$$N_1 = \left(J_a - J_z\right)\left(\Omega^2 - {\Omega_r}^2\right) + M\left(\Omega^2 - {\Omega_t}^2\right){z_1}^2 + 2\sqrt{M\left(J_a - J_z\right)}\ \overline{\Omega}^2 z_1 . \tag{82}$$

We assume $k_{11} \neq 0, k_{22} \neq 0$. It is advantageous to use the following parameters:

stiffness asymmetry

$$\sigma = \frac{k_{12}}{\sqrt{k_{11}k_{22}}} , \tag{83}$$

where

$$-1 < \sigma < 1 , \qquad \overline{\Omega}^2 = \sigma\ \Omega_r\Omega_t ; \tag{84}$$

eccentricity of the balancing device

$$\varepsilon = \sqrt{\frac{k_{11}}{k_{22}}}z_1 ; \tag{85}$$

and rotor-type parameter

$$\mu = \frac{{\Omega_t}^2}{{\Omega_r}^2} = \frac{J_a - J_z}{M}\frac{k_{11}}{k_{22}} . \tag{86}$$

Thus, we obtain

$$\Delta = M \frac{k_{22}}{\Omega_t^2}\left[\left(\Omega^2 - \Omega_t^2\right)\left(\mu\,\Omega^2 - \Omega_t^2\right) - \sigma^2 \Omega_t^4\right], \tag{87}$$

$$N_1 = \frac{k_{22}}{\Omega_t^2}\left[\left(\mu + \varepsilon^2\right)\Omega^2 - \left(1 + \varepsilon^2 - 2\varepsilon\sigma\right)\Omega_t^2\right]. \tag{88}$$

From the condition $\Delta = 0$, we obtain the squares of the critical speeds

$$\Omega_{1,2}^2 = \frac{\Omega_t^2}{2\mu}\left[1 + \mu \pm \sqrt{(1-\mu)^2 + 4\mu\sigma^2}\right], \tag{89}$$

where the lower algebraic sign of the root refers to Ω_1, and the upper sign to Ω_2.
Condition (75) is fulfilled in the following two cases:

Case 1: $\Delta > 0$ and $N_1 > 0$ or (90)

Case 2: $\Delta < 0$ and $N_1 < 0$. (91)

The conditions under Case 1 are identical with the stability conditions of compensatory phasing of two balls each in two planes (see Sperling et al. (2000), Sperling et al. (2001)). They are satisfied, if and only if

$$J_a > J_z, \qquad \Omega > \Omega_2. \tag{92}$$

In the following, additional conditions have to be developed, which result from the conditions under Case 2.

The "long" rotor

The long rotor is defined as one with

$$J_a > J_z, \qquad \mu > 0. \tag{93}$$

Under this condition the rotor has two critical speeds:

$$0 < \Omega_1^2 < \Omega_2^2, \tag{94}$$

and the upper region of stable compensation does exist.
The first condition of (91), $\Delta < 0$, is fulfilled for $\Omega_1 < \Omega < \Omega_2$. The corresponding lower region of stable compensation, $\Omega_1 < \Omega < \Omega_b$, is bounded above by the boundary speed Ω_b, for which we obtain from $N_1 = 0$

$$\Omega_b^2 = \frac{1 + \varepsilon^2 - 2\varepsilon\sigma}{\mu + \varepsilon^2}\Omega_t^2. \tag{95}$$

Because of $|\sigma| < 1$, this expression is always positive:

$$\Omega_b^2 = \frac{\left(1 - |\varepsilon|\right)^2 + 2\left(|\varepsilon| - \varepsilon\sigma\right)}{\mu + \varepsilon^2}\Omega_t^2 > 0. \tag{96}$$

Furthermore,

$$\Omega_1^2 \le \Omega_b^2 \le \Omega_2^2, \tag{97}$$

because of

$$\sigma\,\Omega_t^2 = \operatorname{sgn}\sigma\sqrt{\left(\Omega_t^2 - \Omega_{1,2}^2\right)\left(\Omega_t^2 - \mu\,\Omega_{1,2}^2\right)}, \tag{98}$$

and following from $\Delta = 0$, we obtain

$$N_1 = \frac{k_{22}}{\Omega_t^2}\left[\left(\mu + \varepsilon^2\right)\left(\Omega^2 - \Omega_1^2\right) - \left(\varepsilon\sqrt{\Omega_t^2 - \Omega_1^2} - \operatorname{sgn}\sigma\sqrt{\Omega_t^2 - \mu\,\Omega_1^2}\right)^2\right],$$

$$\Omega_b^{\,2} = \Omega_1^{\,2} + \frac{1}{\mu+\varepsilon^2}\left(\varepsilon\sqrt{\Omega_t^{\,2}-\Omega_1^{\,2}} - \operatorname{sgn}\sigma\sqrt{\Omega_t^{\,2}-\mu\Omega_1^{\,2}}\right)^2 \geq \Omega_1^{\,2}, \tag{99}$$

$$N_1 = \frac{k_{22}}{\Omega_t^{\,2}}\left[\left(\mu+\varepsilon^2\right)\left(\Omega^2-\Omega_2^{\,2}\right)+\left(\varepsilon\sqrt{\Omega_2^{\,2}-\Omega_t^{\,2}}+\operatorname{sgn}\sigma\sqrt{\mu\,\Omega_2^{\,2}-\Omega_t^{\,2}}\right)^2\right],$$

$$\Omega_b^{\,2} = \Omega_2^{\,2} - \frac{1}{\mu+\varepsilon^2}\left(\varepsilon\sqrt{\Omega_2^{\,2}-\Omega_t^{\,2}}+\operatorname{sgn}\sigma\sqrt{\mu\,\Omega_2^{\,2}-\Omega_t^{\,2}}\right)^2 \leq \Omega_2^{\,2}. \tag{100}$$

The eccentricities $\varepsilon=\varepsilon_1$ and $\varepsilon=\varepsilon_2$, for which $\Omega_b^{\,2}=\Omega_1^{\,2}$ and $\Omega_b^{\,2}=\Omega_2^{\,2}$, respectively, result in

$$\varepsilon_1 = \operatorname{sgn}\sigma\sqrt{\frac{\Omega_t^{\,2}-\mu\,\Omega_1^{\,2}}{\Omega_t^{\,2}-\Omega_1^{\,2}}} = \frac{\Omega_t^{\,2}-\mu\,\Omega_1^{\,2}}{\sigma\,\Omega_t^{\,2}} = \frac{1}{2\sigma}\left[1-\mu+\sqrt{(1-\mu)^2+4\mu\sigma^2}\right], \tag{101}$$

$$\varepsilon_2 = -\operatorname{sgn}\sigma\sqrt{\frac{\mu\,\Omega_2^{\,2}-\Omega_t^{\,2}}{\Omega_2^{\,2}-\Omega_t^{\,2}}} = -\frac{\mu\,\Omega_2^{\,2}-\Omega_t^{\,2}}{\sigma\,\Omega_t^{\,2}} = \frac{1}{2\sigma}\left[1-\mu-\sqrt{(1-\mu)^2+4\mu\sigma^2}\right]. \tag{102}$$

The asymmetry $\sigma=\sigma_{1,2}$, for which $\Omega_b^{\,2}=\Omega_1^{\,2}$ ($\sigma=\sigma_1$) or $\Omega_b^{\,2}=\Omega_2^{\,2}$ ($\sigma=\sigma_2$), results from

$$2\varepsilon\sigma-(1-\mu)=\mp\sqrt{(1-\mu)^2+4\mu\sigma^2}$$

as

$$\sigma_{1,2} = \frac{\varepsilon(1-\mu)}{\varepsilon^2-\mu}. \tag{103}$$

If the expression

$$2\varepsilon\sigma-(1-\mu)=\frac{\left(\varepsilon^2+\mu\right)(1-\mu)}{\varepsilon^2-\mu}$$

is positive, $\sigma_{1,2}$ is σ_1, otherwise $\sigma_{1,2}$ is σ_2.

Fig. 7 shows in the $\mu-\varepsilon-$plane all regions for which σ_1 or σ_2, respectively, exist and simultaneously condition (84) is satisfied. We can obtain the σ_1-regions for $\mu<0$ in the same way, because for all parameter values of points in these regions the denominator $\mu+\varepsilon^2$ in Eq. (99) is positive (see Fig. 7).
The significance of Fig. 7 is confirmed also by the parameter values underlying the following figures.

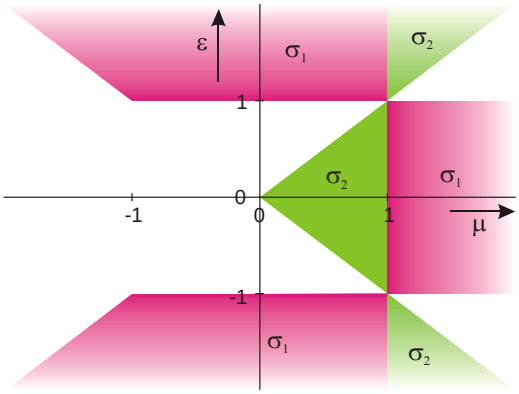

Figure 7. Regions of existence of σ_1 and of σ_2

Illustration in the $\Omega^2-\varepsilon$ coordinate plane

1. Symmetrically supported rotor

With

$$k_{12}=0\rightarrow\overline{\Omega}^2=0\rightarrow\sigma=0 \tag{104}$$

we have

$$\Omega_b^{\,2} = \frac{1+\varepsilon^2}{\mu+\varepsilon^2}\Omega_t^{\,2}, \tag{105}$$

see Figs. 8, 9. For $\varepsilon = 0$, the symmetrically-supported rotor is equipped with the balancing device in the plane of the mass centre. The stability range $\Omega > \Omega_t$ is identical with the one for the plane unbalanced rotor. The vibrations in the central plane are suppressed. If, moreover, the rotor is only statically unbalanced, with compensation in the central plane, then the rotor is completely balanced. A similar situation will occur in the following for $\mu = 0$ and for $\mu < 0$. For $\mu > 0$, in the case of an eccentrically-mounted device two stability ranges always exist.

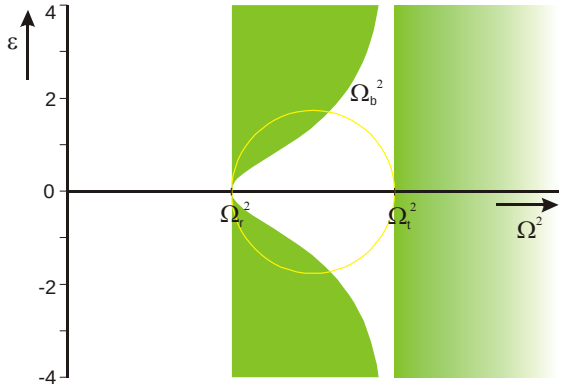

Figure 8. $J_a > J_z$, $\mu = 2$, $\sigma = 0$

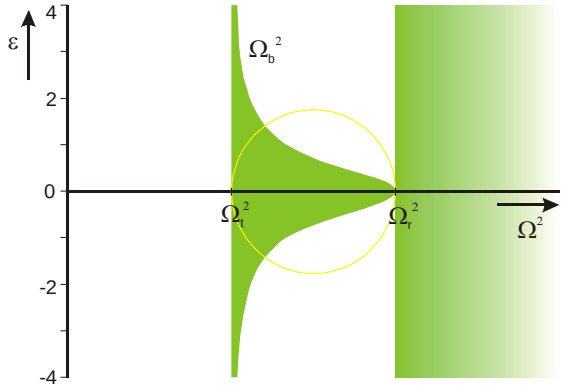

Figure 9. $J_a > J_z$, $\mu = 0.5$, $\sigma = 0$

2. Asymmetrically supported rotor

Because of

$$k_{12} \neq 0 \rightarrow \overline{\Omega}^2 \neq 0 \rightarrow \sigma \neq 0, \tag{106}$$

the boundary speed Ω_b is determined by Eq. (95), see Figs. 10,11. For the eccentricity values ε_1 and ε_2 at each case the two stability ranges are reduced or connected to one stability range.

Illustration in the $\Omega^2 - \overline{\Omega}^2$ or $\Omega^2 - \sigma$ coordinate plane

1. Centrically mounted device

With

$$z_1 = 0 \rightarrow \varepsilon = 0 \tag{107}$$

we have

$$\Omega_b^{\,2} = \frac{\Omega_t^{\,2}}{\mu} = \Omega_r^{\,2}, \tag{108}$$

see Figs. 12,13. For non-vanishing stiffness asymmetry two stability ranges always exist. From the practical point of view, we point to the fact that the borderline case $|\sigma| = 1$ has no practical interest. It will be realised at most approximately.

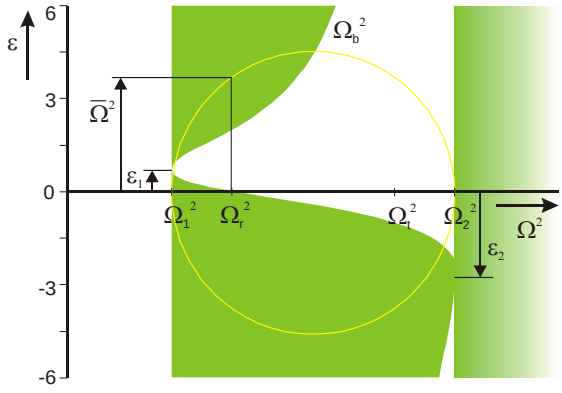

Figure 10. $J_a > J_z$, $\mu = 2$, $\sigma = 0.5$

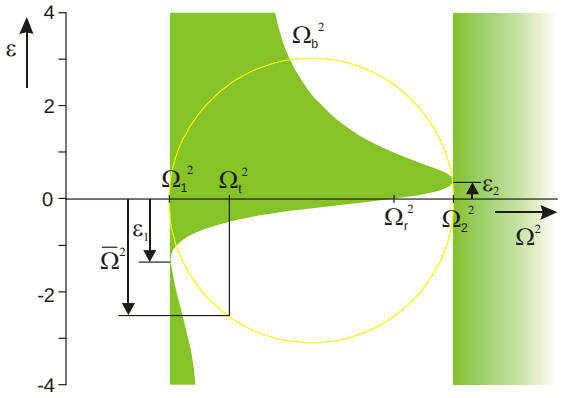

Figure 11. $J_a > J_z$, $\mu = 0.5$, $\sigma = -0.5$

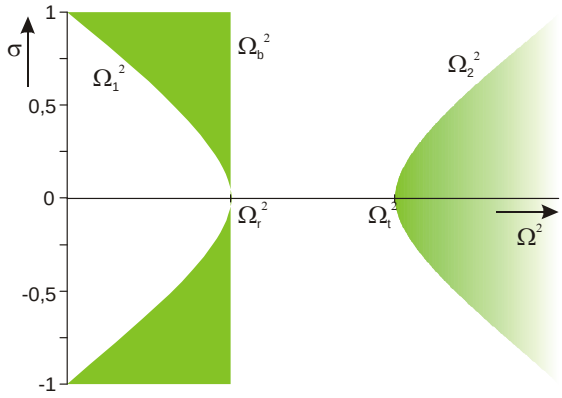

Figure 12. $J_a > J_z$, $\mu = 2$, $\varepsilon = 0$

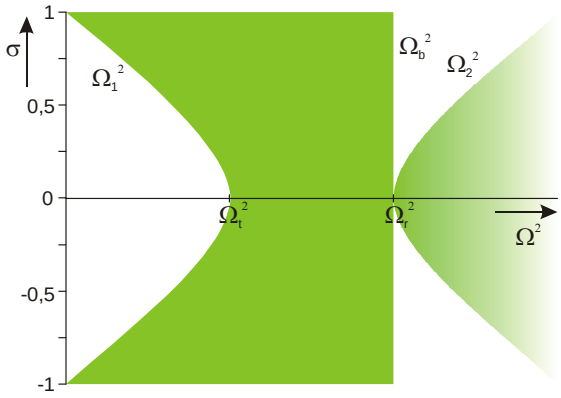

Figure 13. $J_a > J_z$, $\mu = 0.5$, $\varepsilon = 0$

2. Eccentrically-mounted device

With

$$z_1 \neq 0 \rightarrow \varepsilon \neq 0 \qquad (109)$$

the square of the boundary speed can be written as

$$\Omega_b^2 = \Omega_{b0}^2 - \frac{2\varepsilon}{\mu + \varepsilon^2}\sigma\Omega_t^2,$$

$$\Omega_{b0}^2 = \frac{1+\varepsilon^2}{\mu+\varepsilon^2}\Omega_t^2, \qquad (110)$$

$$-1 < \sigma < 1,$$

see Figs. 14-16 and Fig. 7.

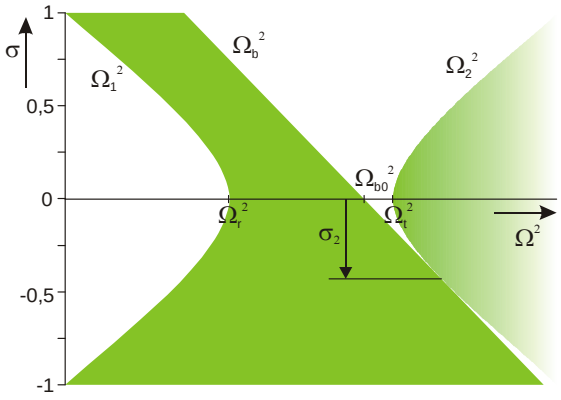

Figure 14. $J_a > J_z$, $\mu = 2$, $\varepsilon = 3$

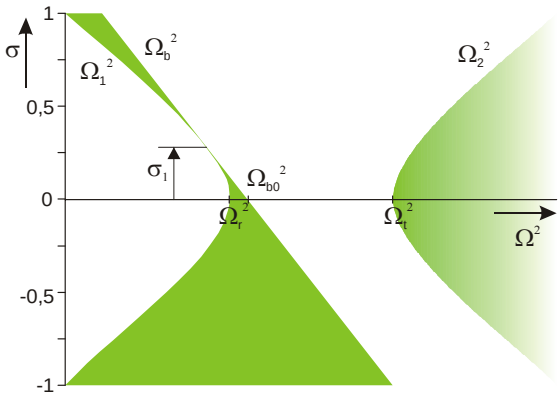

Figure 15. $J_a > J_z$, $\mu = 0.5$, $\varepsilon = 2$

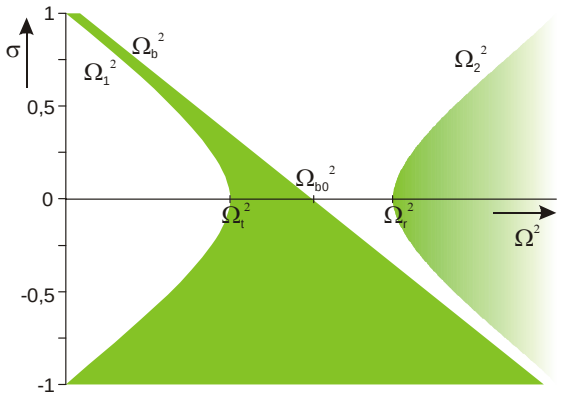

Figure 16. $J_a > J_z$, $\mu = 0.5$, $\varepsilon = 0.7$

The "spherical" rotor

The spherical rotor is defined by

$$J_a = J_z\,, \qquad \mu = 0\,. \tag{111}$$

Eqs. (78), (80), (89) yield

$$\Omega_r{}^2 \to \infty\,, \qquad \overline{\Omega}^2 \to \infty\,, \qquad \Omega_2{}^2 \to \infty\,. \tag{112}$$

From

$$\Delta = Mk_{22}\Omega_t{}^2\left[-\left(\Omega^2 - \Omega_t{}^2\right)\Omega_t{}^2 - \sigma^2\Omega_t{}^4\right] = 0$$

or from

$$\Omega_1{}^2 = \lim_{\mu\to 0}\frac{1}{2\mu}\left[1+\mu-\sqrt{(1-\mu)^2+4\mu\sigma^2}\right]\Omega_t{}^2$$

we obtain the square of the critical speed

$$\Omega_1{}^2 = \left(1-\sigma^2\right)\Omega_t{}^2 \geq 0\,. \tag{113}$$

The boundary speed is determined by

$$\Omega_b{}^2 = \frac{1+\varepsilon^2-2\varepsilon\sigma}{\varepsilon^2}\Omega_t{}^2 = \Omega_1{}^2 + \left(\frac{1}{\varepsilon}-\sigma\right)^2\Omega_t{}^2 \geq \Omega_1{}^2\,. \tag{114}$$

Illustration in the $\Omega^2 - \varepsilon$ coordinate plane

1. Symmetrically-supported rotor

With condition (104) we have the simple formulae

$$\Omega_1 = \Omega_t\,,$$
$$\Omega_b{}^2 = \left(1+\frac{1}{\varepsilon^2}\right)\Omega_t{}^2\,, \tag{115}$$

see Fig. 17.

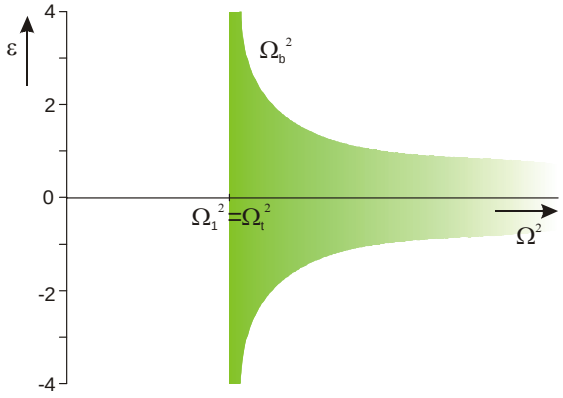

Figure 17. $J_a = J_z$, $\mu = 0$, $\sigma = 0$

2. Asymmetrically supported rotor

For the rotor with non-vanishing stiffness asymmetry, see formula (106), Fig. 18 shows an example for the stability range, where from Eq. (114)

$$\varepsilon_1 = 1/\sigma\,. \qquad (116)$$

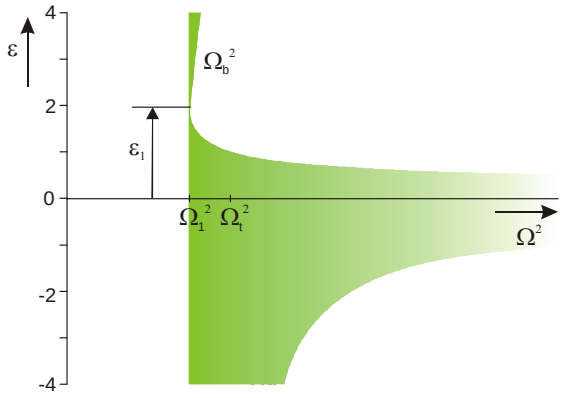

Figure 18. $J_a = J_z$, $\mu = 0$, $\sigma = 0.5$

Illustration in the $\Omega^2 - \sigma$ coordinate plane

1. Centrically-mounted device

With condition (104) we have

$$\Omega_b \to \infty\,, \qquad (117)$$

see Fig. 19.

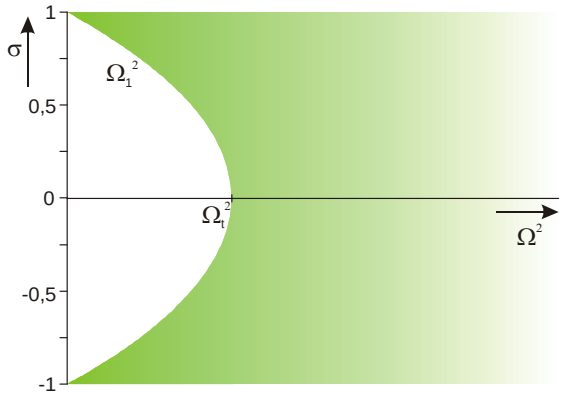

Figure 19. $J_a = J_z$, $\mu = 0$, $\varepsilon = 0$

2. Eccentrically-mounted device

With condition (109) the square of the boundary speed can be written as

$$\Omega_b{}^2 = \Omega_{b0}{}^2 - \frac{2\sigma}{\varepsilon}\Omega_t{}^2,$$

$$\Omega_{b0}{}^2 = \frac{1+\varepsilon^2}{\varepsilon^2}\Omega_t{}^2, \qquad (118)$$

$$-1 < \sigma < 1,$$

see Fig. 20. For the stiffness asymmetry σ_1, for which $\Omega_b = \Omega_1$, we obtain from Eq. (114)

$$\sigma_1 = \frac{1}{\varepsilon}\,. \qquad (119)$$

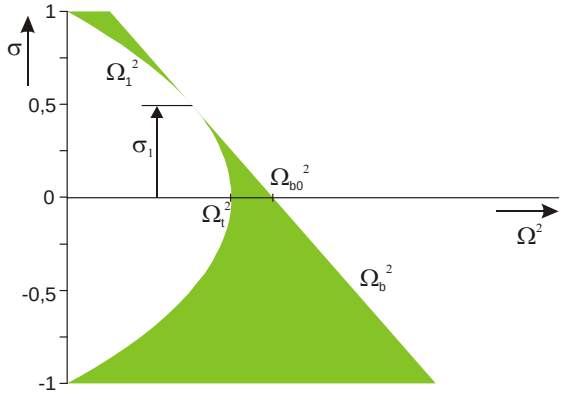

Figure 20. $J_a = J_z$, $\mu = 0$, $\varepsilon = 2$

The "disc-shaft" rotor

The disc-shaft rotor is defined by the condition

$$J_a < J_z\,, \qquad \mu < 0\,. \qquad (120)$$

Eqs. (78) and (89) yield

$$\Omega_r{}^2 < 0\,, \qquad \Omega_2{}^2 < 0\,. \qquad (121)$$

The only critical speed is, see Eq. (89):

$$\Omega_1^2 = \frac{\Omega_t^2}{2\mu}\left[1+\mu-\sqrt{(1-\mu)^2+4\mu\sigma^2}\right] > 0\,. \tag{122}$$

For the boundary speed we obtain from Eq. (95)

$$\Omega_b^2 > \Omega_1^2 \text{ for } \mu+\varepsilon^2 > 0\,,\quad \Omega_b^2 < 0 \text{ for } \mu+\varepsilon^2 < 0\,. \tag{123}$$

Illustration in the $\Omega^2-\varepsilon$ coordinate plane

1. Symmetrically-supported rotor
With condition (104) we have

$$\Omega_1 = \Omega_t,$$
$$\Omega_b^2 = \frac{1+\varepsilon^2}{\mu+\varepsilon^2}\Omega_t^2, \tag{124}$$

see Fig. 21. From Eq. (124), we obtain for Ω_b^2 the asymptotes

$\varepsilon = \sqrt{-\mu}$ and $\varepsilon = -\sqrt{-\mu}$.

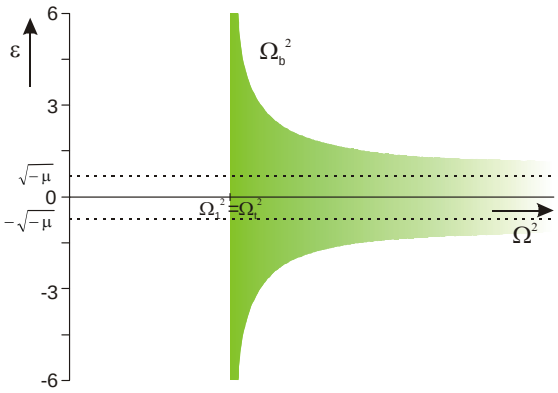

Figure 21. $J_a < J_z$, μ = - 0.5, σ = 0

2. Asymmetrically supported rotor

For the rotor with non-vanishing stiffness asymmetry, see formula (106), Fig. 22 shows an example for the stability range. From Eq. (95), we have the same asymptotes as for the symmetrically supported rotor.

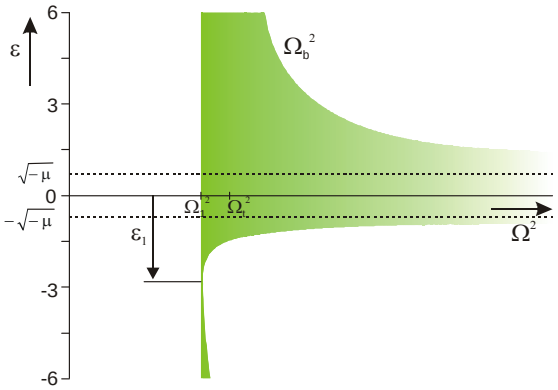

Figure 22. $J_a < J_z$, μ = - 0.5, σ = - 0.5

Illustration in the $\Omega^2-\sigma$ coordinate plane

1. Centrically-mounted device

With condition (107) as for the spherical rotor again Eq. (117) is valid; see Fig. 23.

2. Eccentrically-mounted device

With condition (109) the square of the boundary speed can be written as

$$\Omega_b^2 = \Omega_{b0}^2 - \frac{2\sigma}{\mu+\varepsilon}\Omega_t^2\,,\qquad \Omega_{b0}^2 = \frac{1+\varepsilon^2}{\mu+\varepsilon^2}\Omega_t^2\,,\qquad -1<\sigma<1\,, \tag{125}$$

see Fig. 24 and Fig. 7.

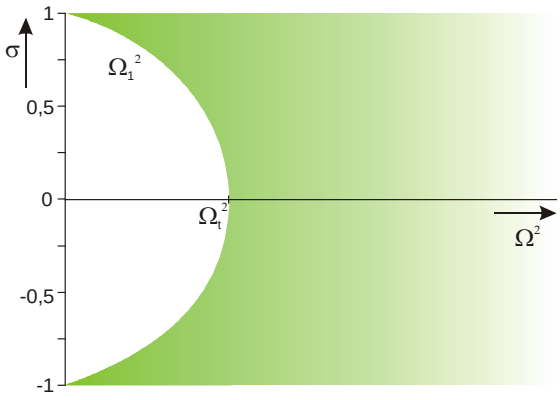

Figure 23. $J_a < J_z$, $\mu = -0.5$, $\varepsilon = 0$

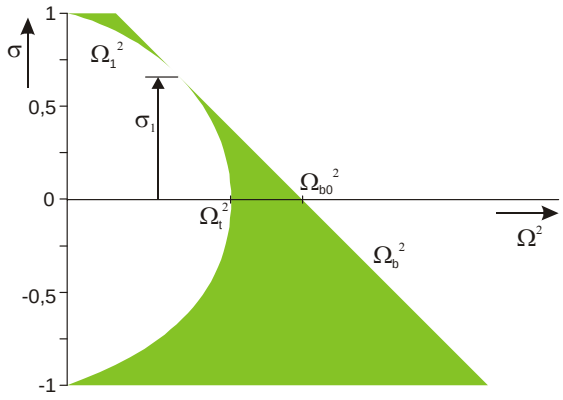

Figure 24. $J_a < J_z$, $\mu = -0.5$, $\varepsilon = 2$

7 Simulation Results

Some simulation results illustrating the processes of unbalance compensation by means of single-plane auto-balancing devices are presented below. Simulations were performed employing the Advanced Continuous Simulation Language (ACSL). We investigated transient processes of rotor run-up to the "nominal" speed higher than critical speeds.

Two rotor systems were considered: "long" ($J_a > J_z$) and "disk-shaft" ($J_a < J_z$). The first rotor system has a mass of 3.15 kg and moments of inertia J_a = 0.0742 kg m^2, J_z = 0.0089 kg m^2. Its critical speeds are 70 rad/s and 135 rad/s; parameters σ = -0.55, μ = 0.68 are close to those, presented in Fig. 11. We used two values of parameter ε: advantageous $\varepsilon = 0.44$ and inauspicious $\varepsilon = -0.44$.

Figs. 25-27 demonstrate the performance of a single-plane auto-balancing device with a single ball for the case of ε = 0.44. Fig. 25 shows the dependence $\kappa_1(\Omega)$. In accordance with condition (51), the condition for decreasing vibrations due to a single-plane self-balancing device with a single ball is

$$-2 < \kappa_1(\Omega) < 0\,. \tag{126}$$

As can be seen from Fig. 25 (the same result follows from Fig. 11), theoretically the area of stable compensatory motion begins beyond the first critical speed, has a small interruption near the second critical speed, and then continues without limitation.

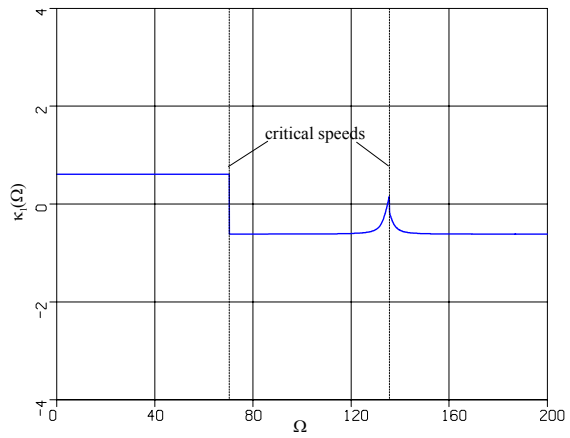

Figure 25. "Long" rotor system. Device with a single ball. Dependence $\kappa_1(\Omega)$ for the case of $\varepsilon = 0.44$.

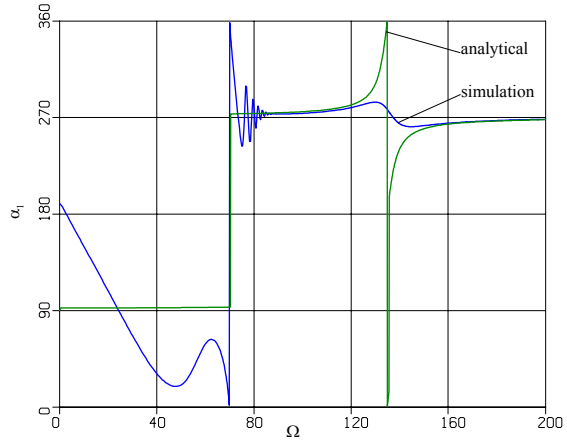

Figure 26. "Long" rotor system. Device with a single ball. Ball angular position for the case of $\varepsilon = 0.44$.

Fig. 26 presents the angular position of the ball during run-up in comparison with the analytical prediction. From the start the ball falls behind the rotor, so the angular position of the ball before the first critical speed does not remain constant. Near the first critical speed we observe a transient process with fast-phase oscillations. This

non-synchronous motion of the balls near the critical speed is of the same nature as the well known Sommerfeld-effect in unbalanced rotor systems with a limited driving moment (Ryzhik et al., 2001 and Ryzhik et al., 2002). Beyond the first critical speed the ball synchronizes with the rotor, providing partial compensation for unbalance. Theoretically, the compensatory phasing may be disturbed near the second critical speed. However, due to the influence of damping, this disturbance in simulations was much smaller than predicted analytically. Fig. 27 shows the amplitude of rotor vibrations in the plane of the device. One can see that for an advantageous choice of parameters the auto-balancing device diminishes vibrations in the region beyond the first critical speed.

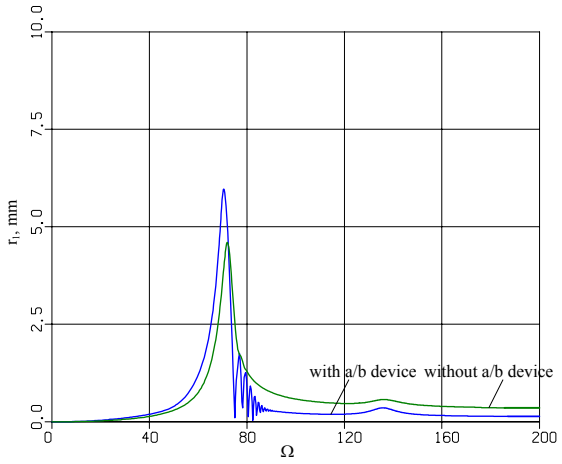

Figure 27. "Long" rotor system. Device with a single ball. Amplitude of rotor vibrations in the plane of the device for the case of $\varepsilon = 0.44$.

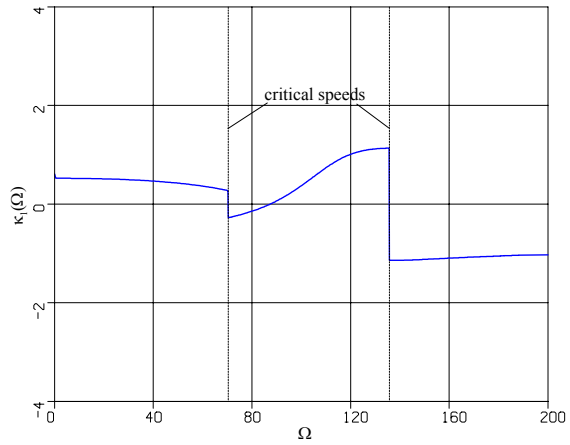

Figure 28. "Long" rotor system. Device with a single ball. Dependence $\kappa_1(\Omega)$ for the case of $\varepsilon = -0.44$.

The results of simulations for the case of $\varepsilon = -0.44$ are presented in Figs. 28-30. Theoretically (Fig. 28), there should be a small area of compensation beyond the first critical speed and an unlimited compensation area after the second critical speed. In simulations we observed only one compensation region, which lies beyond the second critical speed.

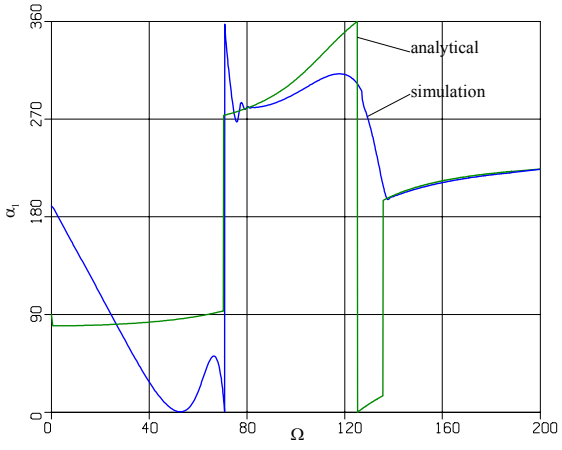

Figure 29. "Long" rotor system. Device with a single ball. Ball angular position for the case $\varepsilon = -0.44$.

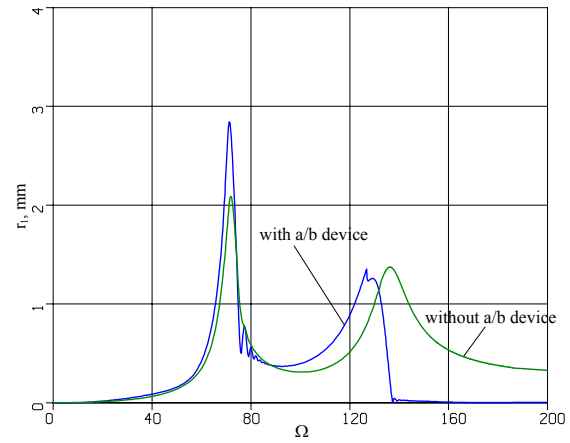

Figure 30. "Long" rotor system. Device with a single ball. Amplitude of rotor vibrations in the plane of device for the case $\varepsilon = -0.44$.

Figs. 31-36 demonstrate the results of simulations for the same rotor system in the case of a single-plane auto-balancing device with two balls. Such a device provides diminishing vibrations in the plane of the device for the condition $\kappa_2(\Omega) < 0$; when $\kappa_2(\Omega) < -1$, vibrations in the plane of the device should be equal to zero, at least theoretically, although in practice there are always some residual vibrations.
For advantageous positioning of the auto-balancing device plane (case $\varepsilon = 0.44$), analytical investigation predicts stable unbalance compensation in the area beyond the first critical speed with a short interruption near the second critical speed, as in Fig. 31.

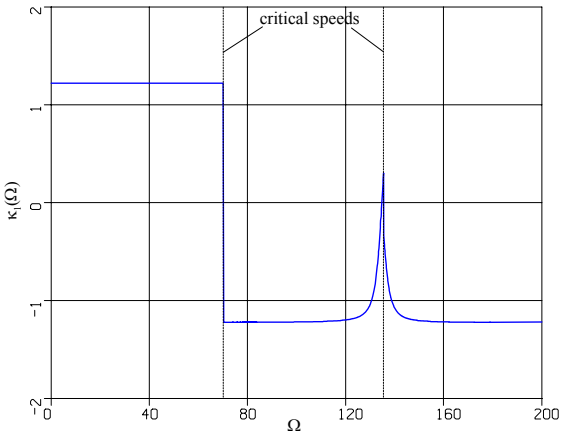

Figure 31. “Long” rotor system. Device with two balls. Dependence $\kappa_2(\Omega)$ for the case $\varepsilon = 0.44$.

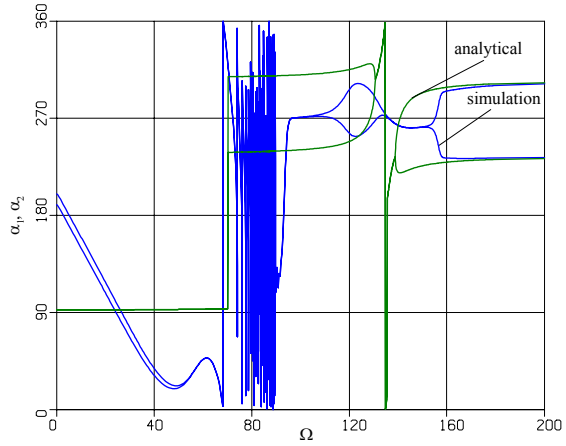

Figure 32. “Long” rotor system. Device with two balls. Ball angular positions for the case $\varepsilon = 0.44$. Low damping.

In simulations we observe a slightly different picture. After passing the critical speeds balls synchronize with the rotor staying theoretically unstable under condition $\kappa_2(\Omega) < -1$ positions $\alpha_1^* = \hat{\alpha}_1$, $\alpha_2^* = \hat{\alpha}_1$ (Figs. 32, 33). Only later, in the area of comparatively high speeds and low accelerations, balls separate and look for the compensatory positions as under (54). The separation point depends mostly on the damping parameters β_i: the lower β_i, the earlier balls separate. On the other hand, low damping may prolong the area of non-synchronous ball motions with increased vibrations near critical speed (see Figs. 34, 35).

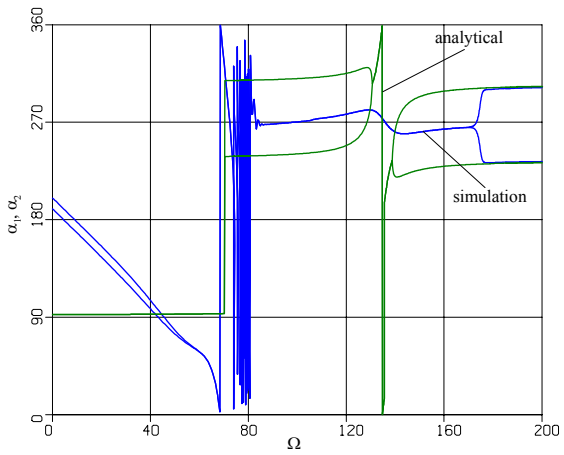

Figure 33. “Long” rotor system. Device with two balls. Ball angular positions for the case $\varepsilon = 0.44$. Rather high damping.

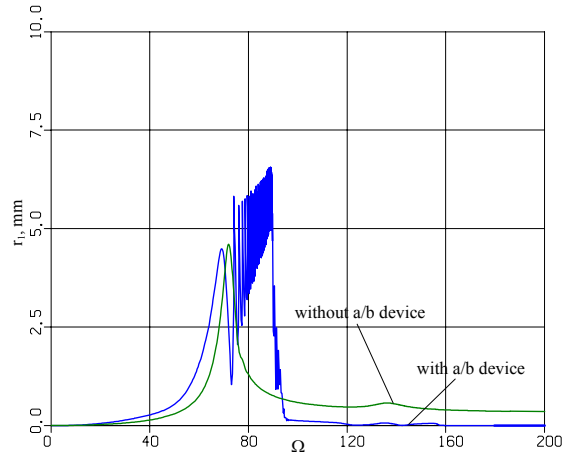

Figure 34. “Long” rotor system. Device with two balls. Amplitude of rotor vibrations in the plane of device for the case $\varepsilon = 0.44$. Low damping.

For the case of ε = -0.44, the compensation area begins after the second critical speed. As above, we observe non-synchronous motion of the balls, this time mostly near the second critical speed, and the region where the balls keep theoretically unstable positions $\alpha_1^* = \hat{\alpha}_1$, $\alpha_2^* = \hat{\alpha}_1$ (Figs. 36-38).

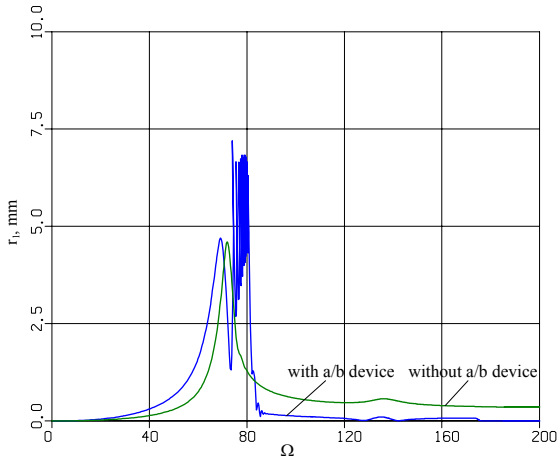

Figure 35. “Long” rotor system. Device with two balls. Amplitude of rotor vibrations in the plane of device for the case $\varepsilon = 0.44$. Rather high damping.

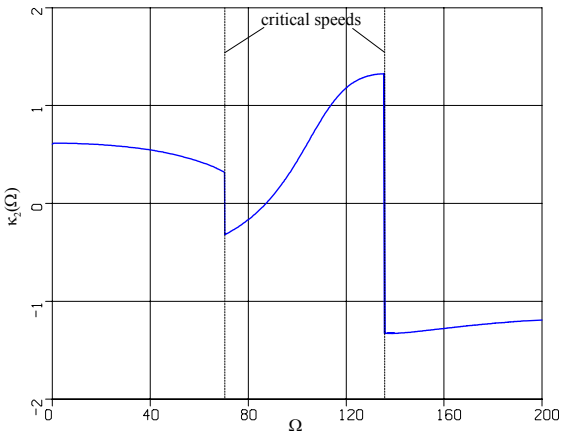

Figure 36. “Long” rotor system. Device with two balls. Dependence $\kappa_2(\Omega)$ for the case $\varepsilon = -0.44$.

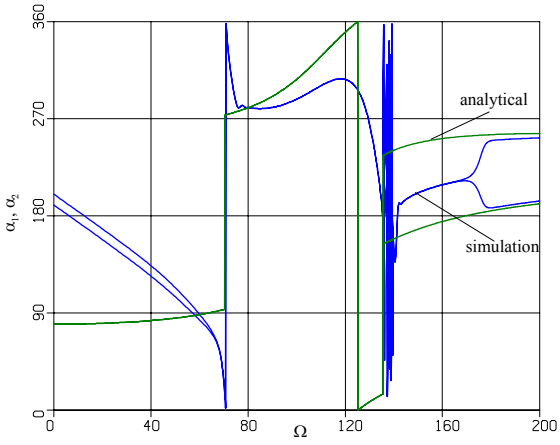

Figure 37. “Long” rotor system. Device with two balls. Ball angular positions for the case $\varepsilon = -0.44$.

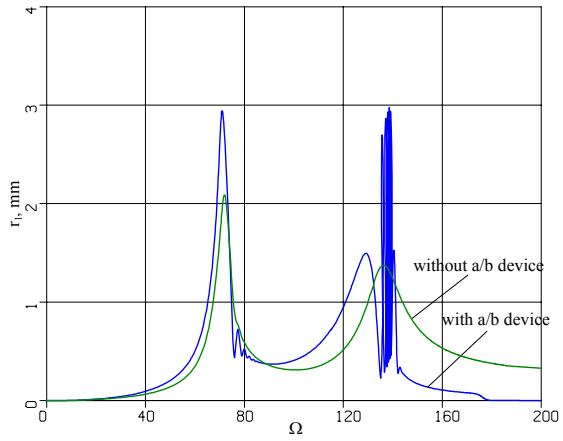

Figure 38. “Long” rotor system. Device with two balls. Amplitude of rotor vibrations in the plane of device for the case $\varepsilon = -0.44$.

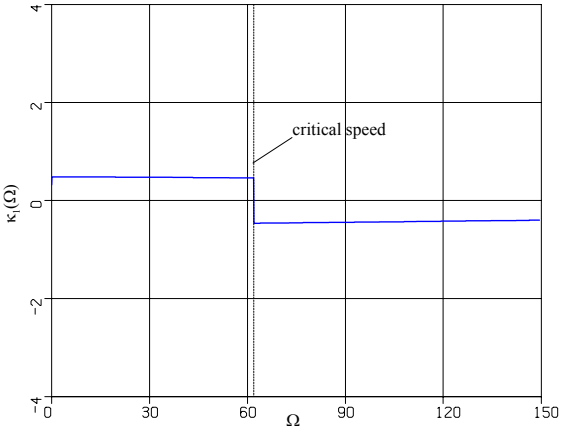

Figure 39. “Disk-shaft” rotor system. Device with a single ball. Dependence $\kappa_1(\Omega)$.

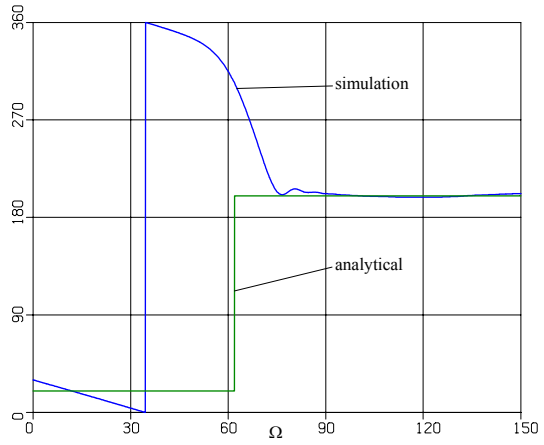

Figure 40. “Disk-shaft” rotor system. Device with a single ball. Ball angular position.

The second "disk-shaft" rotor system has a mass of 12.5 kg and moments of inertia J_a = 0.0936 kg m^2, J_z = 0.1771 kg m^2. Its only critical speed is 62 rad/s; parameters σ, μ are σ = -0.98, μ = -0.78. The stable compensation picture is similar to that presented in Fig. 22. We consider only one value of parameter $\varepsilon = 0.5$, which provides the unlimited area of stable partial compensation in the region beyond the critical speed.

Figs. 39-41 demonstrate the results of computations for a single-plane device with a single ball. The dependence $\kappa_1(\Omega)$ is presented in Fig. 39. As predicted in Fig. 22, the area of stable compensation begins beyond the critical speed and continues without limitation.

The position of the ball and rotor vibrations during run-up are presented in Figs. 40, 41. One can see that after the ball synchronizes with the rotor in the post-critical area the device diminishes the rotor vibrations.

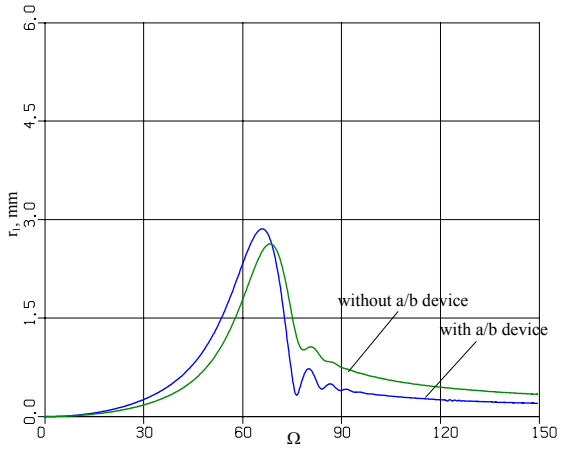

Figure 41. "Disk-shaft" rotor system. Device with a single ball. Amplitude of rotor vibrations in the plane of device.

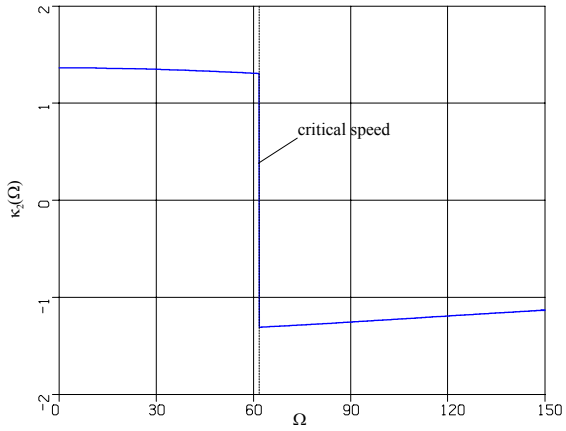

Figure 42. "Disk-shaft" rotor system. Device with two balls. Dependence $\kappa_2(\Omega)$.

Figs. 42-44 demonstrate the performance of a single-plane device with two balls. In this case vibrations in the plane of device in the post-critical area become equal to zero, although in other rotor planes there are some residual vibrations (partial compensation of unbalance). The effects described above of non-synchronous motions near the critical speed and of the theoretically unstable phasing $\alpha_1^* = \hat{\alpha}_1$, $\alpha_2^* = \hat{\alpha}_1$ within a certain range of rotor speeds beyond the critical speed may be clearly observed.

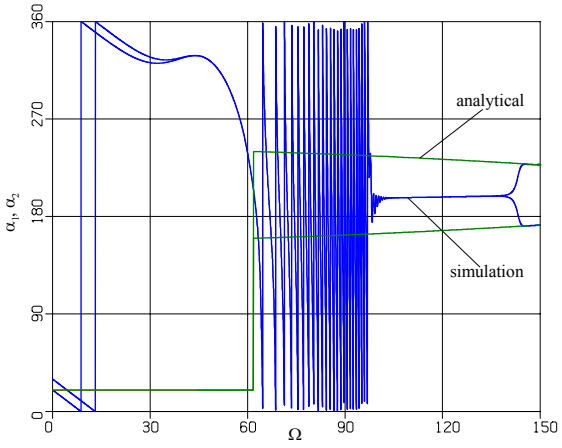

Figure 43. "Disk-shaft" rotor system. Device with two balls. Ball angular positions.

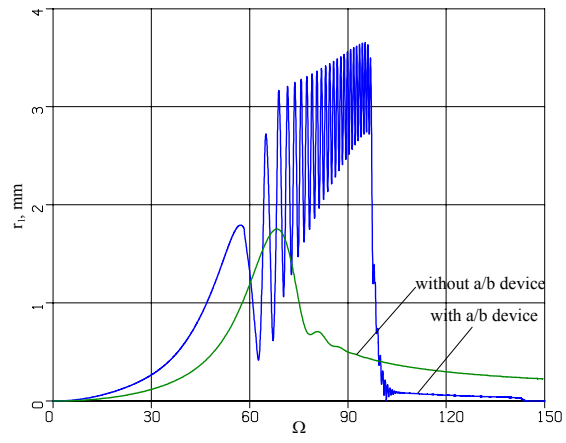

Figure 44. "Disk-shaft" rotor system. Device with two balls. Amplitude of rotor vibrations in the plane of device.

8 Conclusions

Analytical investigations have revealed that, under certain conditions, single-plane auto-balancing devices are suitable for providing partial compensation of static and dynamic unbalances and for reducing vibrations to a major extent. Conditions for a stable partial unbalance compensation have been derived for different types of rotors, including rotors with a polar moment of inertia greater than the transverse one. In particular, the possibility of partial compensation in the frequency range beyond the first critical speed has been revealed.
The analytical conclusions were verified by numerical simulations. Simulations confirm the results presented, but also demonstrate that in the areas near critical speeds the auto-balancing device may engender increased vibrations due to non-synchronous ball motions. To avoid this undesirable effect, it is necessary to carefully select the device parameters.
The possibility of partial compensation considerably extends the potential range of applications of automatic balancing. In future research work the authors intend to investigate a partial unbalance compensation by two-plane auto-balancing devices.

Acknowledgments
The authors would like to express gratitude to the Deutsche Forschungsgemeinschaft for the financial support (No. SP 462/7-3).
The authors are grateful to Professor Mikhail F. Dimentberg, for helpful discussion during his stay in our University as a Fulbright researcher/lecturer. The excellent opportunity for mutual research as provided by the Fulbright Commission is most highly appreciated.

References

Blekhman, I.I.: *Vibrational Mechanics*. World Scientific, Singapore, New Jersey, London, Hong Kong, 2000

Bövik, P.; Högfors, C.: Autobalancing of rotors. *J. of Sound and Vibration* 111, 3, (1986), 429 - 440

Chung, J.; Ro, D.S.: Dynamical analysis of an automatic dynamic balancer for rotating mechanisms. *J. of Sound and Vibration* 228, 5, (1999), 1053 - 1056

Hedaya, M.T.; Sharp, R.S.: An analysis of a new type of automatic balancer. *J. Mechanical Engineering Science*, 19, 5, (1977), 221 - 226

Huang, W.-Y.; Chao, C.-P.; Kang, J.-R.; Sung, C.-K.: The application of ball-type balancers for radial vibration reduction of high speed optic drives. *Journal of Sound and Vibration*, 250, 3, (2002), 415 – 430

Inoue, J.; Jinnouchi, Y.; Kubo, S.: Automatic balancers (In Japanese). *Transactions of the JSME*, Ser. C, 49, (1979), 2142 - 2148

Kang, J.-R.; Chao, C.-P.; Huang, C.-L.; Sung, C.-K.: The dynamics of a ball-type balancer system equipped with a pair of free-moving balancing masses. *Transactions of the ASME*, 123, (2001), 456 - 465

Ryzhik, B., Amer, T., Duckstein, H. and Sperling L.: Zum Sommerfeldeffekt beim selbsttätigen Auswuchten in einer Ebene, *Technische Mechanik*, Vol. 21, No. 4, (2001), 297 - 312

Ryzhik, B., Sperling L. and Duckstein, H.: Display of the Sommerfeld-Effect in a Rigid Rotor One-Plane Autobalancing Device, *Proc. of XXX Summer School "Advanced Problems in Mechanics"*, St. Petersburg (2002), 554 - 563

Sperling, L.; Merten, F.; Duckstein, H.: Self-synchronization and automatic balancing in rotor dynamics. *Int. J. Rotating Machinery* 6, 4, (2000), 275 - 285

Sperling, L.; Ryzhik, B.; Duckstein, H.: Two-plane automatic balancing. *Machine Dynamics Problems*, 25, 3/4, (2001), 139 - 152

Sperling, L.; Ryzhik, B.; Linz, Ch.; Duckstein, H.: Simulation of two-plane automatic balancing of a rigid rotor. *Mathematics and Computers in Simulation*, 58, 4 – 6, (2002), 351 - 365

Thearle, E.L.: A new type of dynamic-balancing machine. *Transactions of the ASME*, 54, 12,(1932), 131 - 141

Address: Prof. Dr.-Ing. habil. Lutz Sperling, Dr.-Ing. Boris Ryzhik and Dr.-Ing. Henner Duckstein, Institut für Mechanik, Otto-von-Guericke Universität Magdeburg, Universitätsplatz 2, 39106 Magdeburg.
E-mail: Lutz.Sperling@mb.uni-magdeburg.de, Boris.Ryzhik@mb.uni-magdeburg.de, Henner.Duckstein@mb.uni-magdeburg.de